Heliyon 10 (2024) e23190

Contents lists available at ScienceDirect

Heliyon

journal homepage: www.cell.com/heliyon

Effect of tin concentrations on the elemental and optical properties of zinc oxide thin films

Adeoye Victor Babalola [a,e,*], Victoria Oluwasusi [e,f], Victor Adewale Owoeye [b], Joseph Onyeka Emegha [c], David A. Pelemo [d], A.Y. Fasasi [d], Umar Milka Gurku [e], Samson Oluwagbemiga Alayande [g], Samson Yusuf [e], Baba Saje M [a]

[a] Nile University of Nigeria, Research and Institution Area, Jabi, Abuja, FCT, Nigeria
[b] Department of Physical and Chemical Sciences, Elizade University, Ilara-Mokin, Nigeria
[c] College of Natural and Applied Sciences, Novena University Ogume, Delta State, Nigeria
[d] Centre for Energy Research and Development, Obafemi Awolowo University, Ile Ife, Nigeria
[e] Department of Physics, Nasarawa State University, Keffi, Nigeria
[f] Department of Physics, Bingham University, Nasarawa, Nigeria
[g] Department of Chemistry, First Technical University, Ibadan, Nigeria

ARTICLE INFO

Keywords:
Thin films
Spray pyrolysis
Semiconductor
Thickness
Composition and Rutherford Backscattering Spectrometry

ABSTRACT

Pure zinc oxide and Sn-doped ZnO thin films were deposited on a pre-heated glass substrate from tin (II) chloride dihydrate ($SnCl_2.2H_2O$) and zinc acetate ($Zn(CH_3COO))_2$ precursors using spray pyrolysis technique. The doped films were achieved by adding various quantities of ($SnCl_2.2H_2O$) precursor to the solution of zinc acetate in volume percent range of 0–10. Rutherford Backscattering Spectrometry (RBS) was used to characterise the prepared films to determine their thickness and elemental composition. To examine the films' optical characteristics, a UV spectrometer operating at room temperature and covering a wavelength range of 300–1100 nm was employed. The film's thickness and composition show that as the volume of Sn in the thin films increases, so does the film's thickness. With average transmittance values up to 70 %, all the films are quite transparent in the visible region of the electromagnetic spectrum and have a significant UV cut-off at roughly 380 nm. The reflectivity of Sn-doped ZnO films is seen to be independent of the volume of Sn in the films, and the reflectivity of the films diminishes as the wavelength increases. Sn-doped ZnO thin film has an optical band gap of 3.14–3.18 eV. The properties of the thin film produced make it suitable for solar energy collection and improve the efficiency of solar energy system, various optoelectronics devices and sensor.

1. Introduction

Semiconductor oxide thin films are materials that find wide uses in optoelectronic and electrical devices, in addition to a few other uses including heat mirrors, protective coatings, and catalysis [1–3]. In the context of the world's energy needs, particularly energy conversion, transparent conductive oxides (TCOs), which are based on semiconductor oxides, are essential to the development of contemporary thin film solar cells. Complex oxides with highly correlated functional characteristics exhibit quantum phenomena like

* Corresponding author. Nile University of Nigeria, Research and Institution Area, Jabi, Abuja, FCT, Nigeria.
E-mail address: babalolaoau@gmail.com (A.V. Babalola).

https://doi.org/10.1016/j.heliyon.2023.e23190
Received 24 February 2023; Received in revised form 27 November 2023; Accepted 29 November 2023
Available online 12 December 2023

multiferroicity, Bose-Einstein condensation of magnons, and high temperature superconductivity with a broad range of peculiar electrical and magnetic phenomena, brought on by the interactions between charge and spin-orbit ordering [4].

High active losses in metal compounds and their alloys due to eddy currents are a serious drawback. This is not a problem for hexaferrites, which have good microwave properties and are dependable in challenging environments [5,6]. Researchers from all around the world are considering the potential uses of ZnO in several innovative devices, making it one among the widely studied transition metal oxides (TMOs). The various multifunctional applications of ZnO are because of its significant energy gap at ambient temperature of 3.37 eV and high 60 MeV exciton binding energy [7–9]. ZnO has recently been used in optoelectronic devices such as photocatalytic degradation, solar cells, gas sensors, photoanodes, and steel anti-corrosion protection [10–14].

The doping of parent materials with additional reinforcing agents is a result of parent metallic oxide's inability to satisfy the required need in industries and engineering. Studies on ZnO have revealed that adding metallic ions into its crystal structure can improve the material's characteristics for various applications [15–24]. Particularly elements with periodic arrangements in III and IV, including Sn, In, Ga, and Al, are suitable for n-type ZnO doping. Previous studies suggested that ZnO's properties depend on preparation processes, morphology, and life conditions change [25]. The addition of a second phase has also been reported to increase the electronic characteristics of the composite materials produced through combining various compounds with excellent electronic properties [26–28]. According to a study by Ref. [29], Ni/Zn/Fe_2O_4 (NZF)-$BaTiO_3$ (BT) could have their electrical and conductivity properties improved by growing NZF at the nanoscale on top of or in between microscale BT. Because of the composite materials' observable properties, they can be used in ceramic supercapacitors, tunable frequency filters, and high-frequency microwave devices.

The synthesis of nanostructured Sn-doped ZnO via hydrothermal process for dye sensitized solar cells was the focus of [17], the study also examined the doped ZnO's photovoltaic capabilities. By arranging the tiny ZnO nanoparticles, the dopant was said to change the morphology of ZnO into a spindle shape. It was found that adding a Sn atom to the ZnO nanostructure increased conversion effectiveness and photocurrent density, which may have benefited the high charge collection and electron transport at the interfaces between the electrolyte and doped zinc oxide layers.

The preparation of undoped and Sn–ZnO nanoparticles for magnetic applications is the focus of the study [25]. Sn doped ZnO nanoparticles were discovered to have hexagonal wurtzite structure, with a minimum crystal size of approximately 32.7 nm. With an increase in Sn doping concentration, it was shown that the quantity of defects and catalyst formed in ZnO both increased. Sn doped ZnO nanoparticles were found to exhibit greater saturation magnetization at room temperature because of the annealing effect. ZnO was synthesized using a conventional chemical precipitation process and doped with a transition metal (Sn) in Ref. [30]. Addition of Sn atom to the ZnO crystal structure caused the lattice gap to increase and the 2 angle to decrease.

Research study [31] focused on the antibacterial and photocatalytic properties of Sn–ZnO nanoparticles prepared using precipitation method. Increased Sn concentration was shown to increase crystallite size and reduce lattice parameter without altering the zinc oxide structure. The optical reflectance and band gap of Sn doped ZnO were decreased as the dopant concentration was increased. In comparison to the 3 % Sn, 5 % Sn doped ZnO nanoparticles showed a higher dye removal rate for methylene blue. The Sn doped ZnO's antibacterial activity shown an increased inhibition of roughly 14×10^{-3} m against various pathogens. The photocatalyst of 5 % Sn–ZnO increases photo excite carrier transfer rate and decreases recombination rate, may significantly influence the photocatalytic performance. Other complex oxide groups, including FeCo/Fe2CoO4/Co3O4, were also revealed to have exceptional electrical properties and could be utilized as anode materials for lithium-ion batteries [32]. New materials with enhanced and appealing electrical properties could be produced by mixing various types of polymers with nanoparticle ceramic fillers [33,34].

Both top-down and bottom-up approaches can be used to nanostructure materials. Top down involves transforming a bulk material into a nanostructured material. Different severe plastic deformation techniques, like extrusion, drawing, rolling, equal channel angular extrusion, and others, are used in this process [35]. The second approach means developing nanostructured materials from the atom up, and the thin-film method of doing so falls under this category [10,15,16,36]. A material with a thin layer is one whose thickness is between one and one hundred nanometers, or less than 1 μm [36].

Synthesis of metal/semiconductor oxide thin film has been done by various techniques including, electrochemical deposition method [27,28], sol–gel spin-coating technique [37–39], spray pyrolysis [10,12,15,16], molecular beam epitaxy [40], metalorganic chemical vapour deposition [41], pulsed laser deposition [42], co-precipitation technique [29,43], electrodeposition [44],

Due to its many advantages over other deposition techniques, including its ability to adjust to a wide range of deposition parameters, its low power consumption, and its affordability, spray pyrolysis technique (SPT) was chosen as the thin film deposition technique used in this study [45–47]. Thin film technology is essential for materials research since materials exhibit distinctiveness in each of their properties at the nanoscale, including morphology, microstructure, electrical, thermal, optical, magnetic, anti-corrosion, and mechanical properties [10,15,16].

A review of the literature showed limited publications on the study of thickness and elemental composition of Sn/ZnO thin film for optoelectronic applications using Rutherford Backscattering Spectrometry (RBS). We present the synthesis of Sn:ZnO thin films via SPT in this work, as well as the physical characterization of the resulting films. To determine the ideal conditions for the deposition process, the influence of Sn concentrations on the thickness, elemental composition, and optical characteristics of these films was examined.

2. Experimental

Zinc acetate was used to synthesize the precursor for zinc oxide and tin oxide from tin (II) chloride dihydrate ($SnCl_2.2H_2O$) precursor, both were dissolved in methanol at 0.01 M and 0.05 M. The choice of the zinc salt over other precursors' salts like zinc chloride, zinc nitrate and zinc sulfate has been reported by Refs. [15,16,24]. Undoped films of ZnO were deposited separately on a glass substrate and characterised. Sn-doped ZnO were achieved by adding various quantities of ($SnCl_2$. $2H_2O$) to the solution of zinc acetate

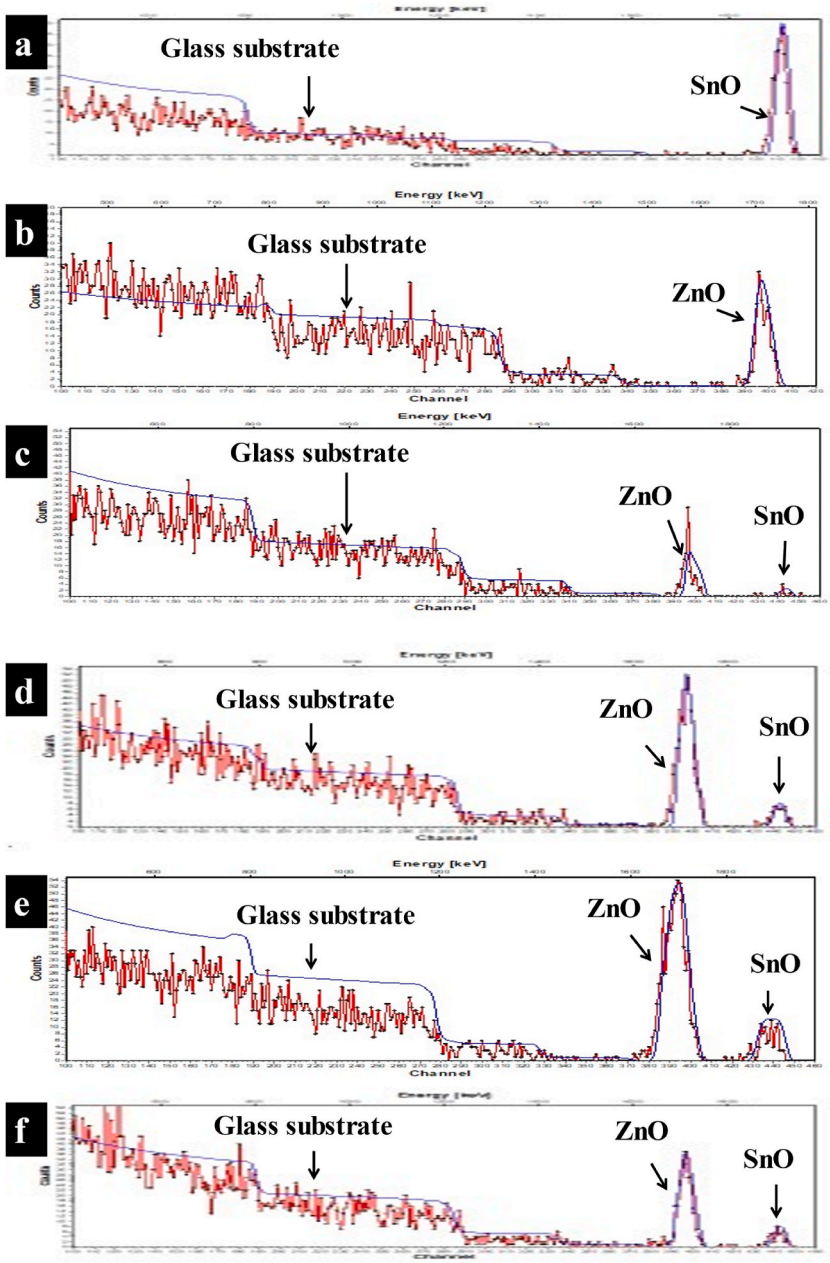

Fig. 1. RBS Spectra of (a) ZnO (0.05 M) (b) 0.05 M SnO and (c) 4 % Sn-doped ZnO 0.05 M RBS Spectra of Sn-doped ZnO 0.05 M (d) 6 % dopant (e) 8 % dopant, and (f) 10 % dopant.

solution in volume percent range of 0–10. Using the methods previously employed in Refs. [15,16,24], the amount of the dopant was determined as a function of the desired Sn/Zn ratio. Chemical spray pyrolysis technique (SPT) was used to pyrolyze the prepared precursor and deposit thin films on a clean glass substrate at 350 °C. Deposition temperature was monitored with a thermocouple.

Characterisations were carried out using RBS to examine the composition and thickness of the films. The samples were analysed using 2 MeV He^{+} tandem electrostatic ion accelerators with 0.3 μC. The data were collected electronically and analysed using dedicated software called SIMNRA [15]. A UV-1800 Spectrophotometer operating at room temperature and covering a wavelength range of 300–1100 nm was used for evaluating optical measurements of the films.

Table 1
SnO, ZnO, and Sn-doped ZnO thin film composition & thickness.

Thin film	Sn	Zn	O	Thickness (nm)
0.05 M SnO	0.101592	–	0.898408	65.66
0.05 M ZnO	–	0.539630	0.460370	63.96
4 % Sn–ZnO 0.05 M	0.011351	0.293571	0.695078	45.84
6 % Sn–ZnO 0.05 M	0.023886	0.525646	0.450468	74.92
8 % Sn–ZnO 0.05 M	0.021379	0.247403	0.731218	97.56
10 % Sn–ZnO 0.05 M	0.014999	0.237111	0.747890	78.87

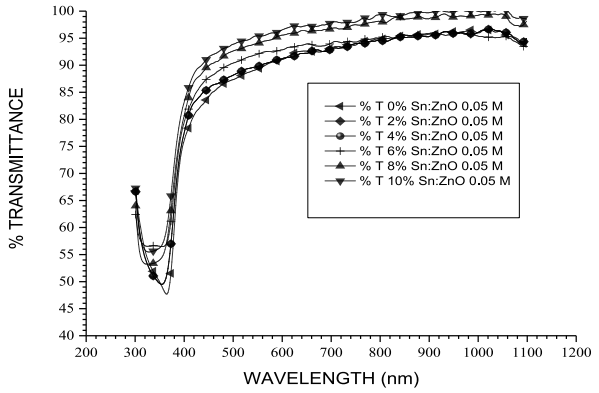

Fig. 2. Optical transmittance of 0.05 M Sn–ZnO thin films.

3. Results and discussion

3.1. Film's thickness and stoichiometry

The RBS spectra of ZnO, Sn-doped ZnO, and undoped 0.05 M SnO films are displayed in Fig. 1(a–f). The experimental RBS data was fitted with SIMNRA software, and the thickness and composition of the films were determined. For ion beam analysis using MeV ions, SIMNRA is a suitable Microsoft Windows tool for simulating back- or forward-scattering spectra. As a result, it is mostly used to simulate spectra with nuclear processes, elastic recoil detectors, non-RBS, or EBS cross sections. The application fits the data (layer roughness, thickness, energy calibration, and layer composition) using the Simplex algorithm, which is very stable and converges slowly but almost always. The RBS analysis of the films was conducted using this software.

The RBS results confirmed the synthesis of Sn, Zn and Sn–ZnO films as evident from the RBS spectra showed in Fig. 1 and Table 1 respectively. The two peaks detected by the RBS in Fig. 1(c–f) confirmed the successful substitution of Sn^{4+} ion into the zinc oxide crystal lattice. The substitution reaction is enhanced by the variation in the ionic radius between Sn^{4+} (0.69 Å) and Zn^{2+}(0.74 Å). The elemental compositions and thickness of the films shown in Fig. 1 were analysed by SIMNRA with the results presented in Table 1. According to the elemental analysis, the percentage of 0.05 M SnO is Sn: 10.16 % and O: 89.84 % with 65.66 nm thickness while that of 0.05 M ZnO are in proportion of Zn: 53.96 % and O: 46.04 % with 63.96 nm thickness.

The deposited thin films of 0.05 M Sn-doped ZnO on glass substrate reveals that the thickness increases with increased volume of Sn in the thin films except for the suspicious behaviour of 8 % Sn doped film which shows high thickness value which then makes 10 % Sn doped thickness values look as if it decreases as shown in Table 1. The drop in ZnO thickness from 8 to 10 % Sn dopant may have resulted from contamination of the films with impurities during preparation and characterization. Although the thickness values reported by RBS in this investigation are consistent with the conclusion reached in Ref. [48], it is expected that the thickness would increase as the amount of dopants in Sn-doped ZnO increases. The substitution reaction of the Sn atom into the ZnO crystal structure causes the ZnO thickness to rise with increased Sn dopant. The vacant sites in ZnO are filled with Sn atoms because of the substitution reaction caused by the variation between Sn and Zn's ionic radii, which reduces the amount of crystal defect in the Sn–ZnO crystal structure.

The elemental composition for 0.05 M Sn-doped ZnO thin film are as follows: 4 % Sn-doped ZnO are 1.14 %, 29.36 % and 69.51 % for Sn, Zn and O, respectively and for 6 % Sn-doped ZnO are 2.39 %, 52.56 % and 45.05 % for Sn, Sn, and O, respectively and for 8 % Sn-doped ZnO are 2.14 %, 24.74 % and 73.12 % for Sn, Zn and O, respectively, and for 10 % Sn-doped ZnO are 1.50 %, 23.71 % and 74.79 % for Sn, Zn and O, respectively. The noticeable characteristic in the RBS result at 8–10 % Sn-doped ZnO may possibly be caused by air and other impurities contaminating the films after deposition, which causes the Sn concentration to decrease rather than rise with increased Sn content in the Sn-doped ZnO lattice. From Table 1 above, it was observed that the oxygen stoichiometry of the deposited films easily allows the excess composition of oxygen compared to the zinc and tin contents in the samples, Oxygen content had been reported to be proportional to the stoichiometric [49,50].

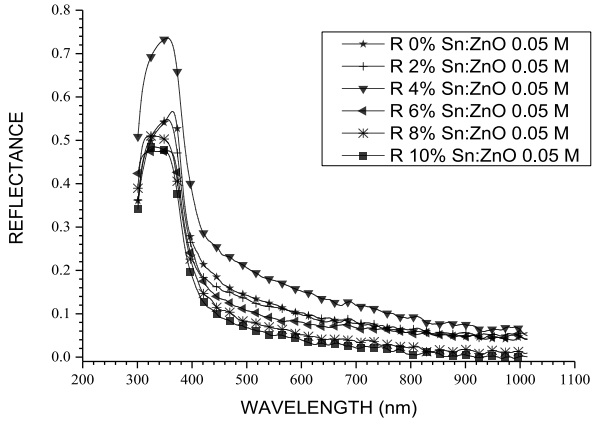

Fig. 3. The reflectivity of 0.05 M Sn-doped ZnO thin films.

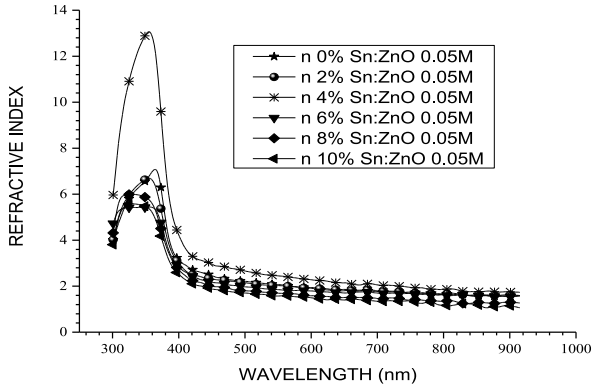

Fig. 4. The refractive index of 0.05 M Sn-doped ZnO.

3.2. *Optical analysis of 0.05 M Sn-doped ZnO*

The optical characteristics of Sn/ZnO films are among the crucial characterizations to determine the nature of semiconducting materials for device applications. The transmittance of 0.05 M Sn– ZnO thin films is shown in Fig. 2. With average transmittance values up to 70 %, all the films (Fig. 2) show a sharp ultraviolet cut-off at about 380 nm and are highly transparent in the visible portion of the electromagnetic spectrum. The results agree with the work of [51], which suggests that the produced films have good optical quality due to low scattering or absorption losses [52].

The deposited nano-films are suitable as an aesthetically pleasing window glazing material due to their excellent transmittance in the visible region [52,53]. Additionally, the film's high transmittance makes it appropriate for lowering solar radiation reflection, solar energy collection, and sending radiation photons to the collector [53]. The behaviour of Sn doped ZnO at wavelengths ($\lambda < 400$ nm) has a great application in such a way that the film can be used as UV-wavelength absorber for the wavelength less than 400 nm.

The films' reflection spectrum is presented in Fig. 3. It was observed that the reflectivity of Sn–ZnO films is independent of the volume of Sn in ZnO films, and the film reflectivity decreases with increase in wavelength. Usually, the films exhibited low reflectance values that lie between 0 and 0.8. Higher reflectivity was observed at around 360 nm and this spontaneously decreases with increase in wavelength, this could be caused by the film's density reducing as tin concentrations rise [27]. The low reflectivity values of the deposited material make tin-doped-zinc oxides thin films good material for anti-reflective coatings [53,54].

The refractive index (n) of thin films is an important optical property that is closely related to the electronic polarizability of ions and the local field within materials. Several optoelectronic devices such as solar cells, modulators, switches, waveguides, filters, detectors, etc, are based on the optical refractive index [55]. Equation (1) was utilized to estimate the refractive index of Sn:ZnO thin films [54–56].

$$n = \frac{-(R+1) \pm \sqrt{3R^2+10R-3}}{2(R-1)} \tag{1}$$

Fig. 4 shows the Sn-doped ZnO thin film's refractive index (n) against wavelength. The result demonstrates that the thin film first increases with the wavelength and then decreases after reaching a maximum value in the range of 300 nm–380 nm which could be

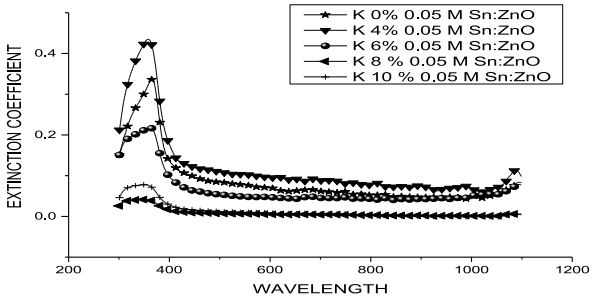

Fig. 5. The extinction coefficient of 0.05 M Sn–ZnO.

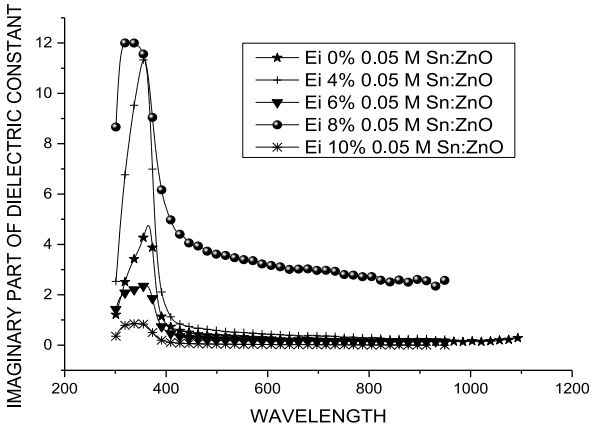

Fig. 6. Imaginary part of the dielectric constant of 0.05 M Sn-doped ZnO thin film.

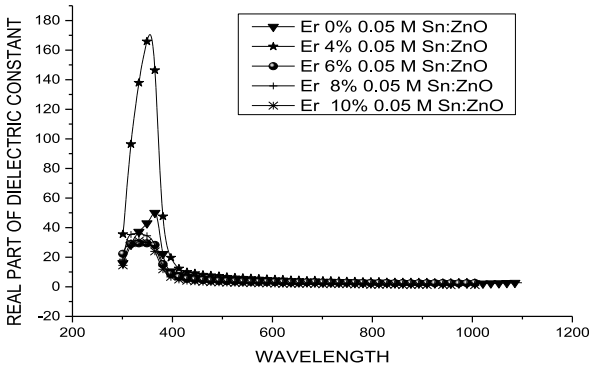

Fig. 7. Real part of the dielectric constant of 0.05 M Sn–ZnO film.

compared with the study of [57], where the ZnO film's refractive index first rises with wavelength and then falls after reaching a maximum in the 380–420 nm wavelength region.

Also, it is observed that the refractive index of the Sn–ZnO thin film is independent on the volume of tin in the deposited thin films. The cause of the increased refractive indexes of deposited thin films is suggested to be the deposition conditions, which agrees with the works of [53,58].

For Sn–ZnO, the extinction coefficient (k) was estimated using the relation in Equation (2) [56].

$$k = \frac{\alpha\lambda}{4\pi} \tag{2}$$

where λ and α are wavelength and the absorption coefficient of the material. The extinction coefficient of the thin films is shown in Fig. 5. The plot shows that the extinction coefficient decreased with wavelength. Furthermore, the overall decrease in extinction coefficient can be likened to the degree of crystallinity of the films as the tin (Sn) content increases. Commonly, the ranges of the

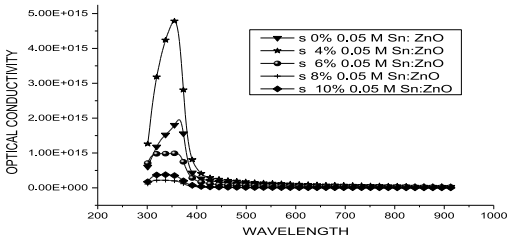

Fig. 8. The optical conductivity of 0.05 M Sn-doped ZnO.

estimated extinction coefficients were somewhat low along the wavelength regions, thus, losing some absorption energy within the wavelength regions [56].

A fundamental characteristic of any optical material, the dielectric constant is correlated with the values of the deposited substance's extinction coefficient and refractive index [52,56]. The real (ε_r) and imaginary (ε_i) parts of Sn–ZnO dielectric constant were determined using Equation (3) and equation (4) [56].

$$\varepsilon_r = n^2 - k^2 \tag{3}$$

and

$$\varepsilon_i = 2nk \tag{4}$$

The variations of the dielectric constant of the deposited materials are depicted in Figs. 6 and 7. It was observed from Figs. 7 and 8 that the dielectric constants (real and imaginary) were decreasing with increase in wavelengths. The figures also made it evident that the real and imaginary dielectric constants have different values. This is because, as Equation (3) shows, the real dielectric constant depends on the refractive index [56]. Similar development was reported in Ref. [56] for chalcogenide thin films.

The optical conductivity (σ) of the samples was evaluated using Equation (5) [54].

$$\sigma = \frac{\alpha n c}{4\pi} \tag{5}$$

where c = speed of light. The films' optical conductivity increased rapidly and get to a peak at 375 nm and starts decreasing (Fig. 8). Increasing the tin (Sn) concentrations has revealed a notable enhancement of the deposited material's optical properties. It was found that the presence of Sn dopant reduced the ZnO crystal structure's barrier height, which increased ZnO's conductivity. When a new Sn atom is added to the ZnO crystal lattice, the improvement further suggests that there are no crystal defects present. According to reports, dopants, or combinations of several compounds with good electrical properties result in novel composite materials that have attracted a lot of interest from the technology community recently. Incorporating an additional phase can greatly increase the electrical properties of the composite material [15,16,29,59]. Different polymer types could also be combined with ceramic nanoparticle fillers to develop novel materials with enhanced and appealing electrical characteristics [33,34]. The difference between the values of the optical conductivities shows that the Sn–ZnO thin films depended largely on the impurity concentration.

The optical band gap of Sn-doped ZnO was determined using the relation in Equation (6) [55].

$$\alpha = \frac{B}{h\upsilon}[h\upsilon - Eg]^n \tag{6}$$

where E g, α, B, and $h\upsilon$ are the band gap, absorption coefficient, proportionality constant, and photon energy respectively. The plot of (α^2) against ($h\upsilon$) for Sn-doped ZnO thin films is depicted in Fig. 9. Given that the films are produced using a direct band gap material [60,61], extrapolating the linear portion (Fig. 9) to the x-axis zero gives the E g. The E g values obtained were found to be 3.17, 3.18, 3.14, 3.17 and 3.15 eV for 0–10 % Sn-doped ZnO thin films. The estimated result is smaller than the values for Sn-doped ZnO thin films reported in Ref. [60], but higher than the value obtained in Ref. [62]. However, the obtained values in this study show that it obeys the Vegard rule of mixture [63]. Different factors may cause the variation in optical band gaps as tin content is added to ZnO thin films. Generally, optical band gaps in semiconducting materials are mostly influenced by the impurities level, grain boundary, heat treatment, structural defects as well as crystallinity [63–65]. According to study [65], irradiation-induced changes in grain size can significantly affect changes in structural and optical properties. Deformation of the crystalline structure and a decrease in crystallite size suggest a change in the dislocation density of defects, which rises due to grain fragmentation, along with their reorientation and the formation of new grain boundaries. It was reported that the main cause of the changes in band gap was the occurrence of new imperfections and porous inclusions in the near-surface layer, which led to the emergence of more absorption centers. The electrical structure of the near-surface layer is influenced by the processes of defect emergence and electron redistribution due to irradiation, which influences the band gap [65]. As a result, the Sn–Zn–O system's impurity levels and the deposition technique used to produce this film can be used to explain changes in energy gap values [54,55].

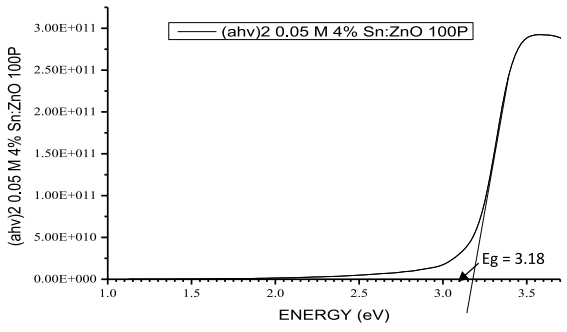

(a)

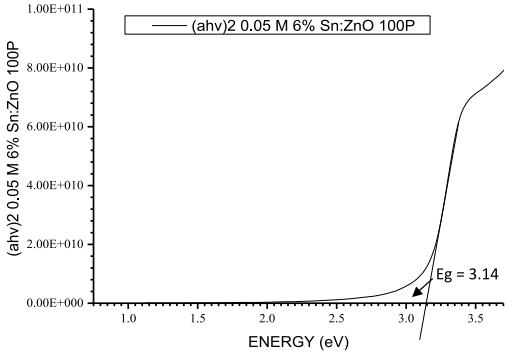

(b)

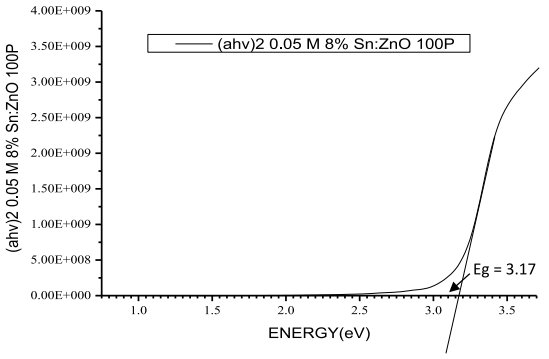

(c)

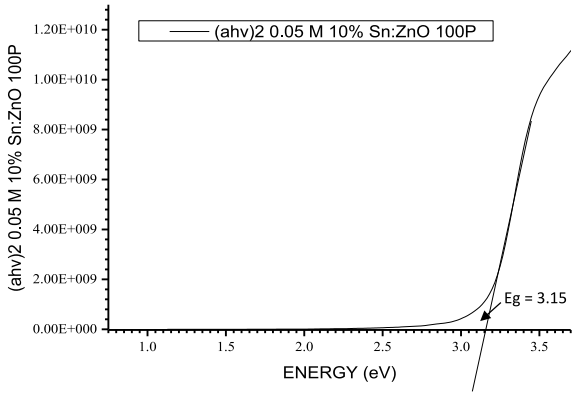

(d)

(caption on next page)

Fig. 9. The Optical Band Gap of 0.05 M Sn-doped ZnO thin film for 4 %, 6 %, 8 % and 10 %.

Table 2
The band gap of Sn-doped ZnO.

		Band Gap				
Material	Condition	% Sn				
Sn-doped ZnO		0	4	6	8	10
0.05 M	As-deposited	3.17	3.18	3.14	3.17	3.15

Sn-doped ZnO thin film has an optical band gap of 3.14–3.18 eV [Table 2].

4. Conclusions

ZnO and Sn:ZnO thin films were deposited on glass substrates using SPT. The samples were characterised using RBS for thickness and elemental composition determination. The presence of Sn, Zn and Sn-doped ZnO were all confirmed in the deposited films. It was observed that ZnO films' thickness increases with increased Sn dopant except for the suspicious behaviour of 8 % Sn-doped film. The transmittance of the films in the electromagnetic spectrum is around 70 % and above which agrees with the optical property of ZnO thin film, and the refractive index of the Sn-doped thin film is independent on the volume of Sn in the deposited thin film.

Data availability statement

The datasets collected for this study are not available to the public, however they can be obtained from the corresponding author upon reasonable request.

CRediT authorship contribution statement

Adeoye Victor Babalola: Writing – review & editing, Writing – original draft, Methodology, Formal analysis. **Victoria Oluwasusi:** Writing – review & editing, Conceptualization. **Victor Adewale Owoeye:** Visualization, Validation, Formal analysis, Data curation. **Joseph Onyeka Emegha:** Writing – original draft, Formal analysis. **David A. Pelemo:** Writing – review & editing, Conceptualization. **Umar Milka Gurku:** Writing – review & editing, Conceptualization. **A.Y Fasasi:** Writing – review & editing, Conceptualization. **Samson Oluwagbemiga Alayande:** Writing – review & editing, Conceptualization. **Samson Yusuf:** Writing – review & editing, Conceptualization. **Baba Saje M:** Writing – review & editing, Conceptualization.

Declaration of competing interest

The authors declare that they have no known competing financial interests or personal relationships that could have appeared to influence the work reported in this paper.

Acknowledgements

The authors acknowledge the immense contribution of all our teachers and lecturers.

References

[1] C.G. Granqvist, Transparent conductors as solar energy materials: a panoramic review, Sol. Energy Mater. Sol. Cells 91 (No. 17) (2007) 1529–1598, https://doi.org/10.1016/j.solmat.2007.04.031.
[2] G.J. Exarhos, X.-D. Zhou, Discovery-based design of transparent conducting oxide films, Thin Solid Films 515 (No. 18) (2007) 7025–7052, https://doi.org/10.1016/j.tsf.2007.03.014.
[3] S. Malato, P. Fernández-Ibáñez, M.I. Maldonado, J. Blanco, W. Gernjak, Decontamination and disinfection of water by solar photocatalysis: recent overview and trends, Catal. Today 147 (No. 1) (2009) 1–59, https://doi.org/10.1016/j.cattod.2009.06.018.
[4] A.V. Trukhanov, et al., Influence of the charge ordering and quantum effects in heterovalent substituted hexaferrites on their microwave characteristics, J. Alloys Compd. 788 (2019) 1193e1202.
[5] Trukhanov, et al., Magnetic and absorbing properties of *M*-type hexaferrites BaFe12 – *x*Ga*x*O19 ($0.1 < x < 1.2$), J. Exp. Theor. Phys. 123 (3) (2016) 461–469, https://doi.org/10.1134/S1063776116090089.
[6] S.V. Trukhanov, A.V. Trukhanov, V.G. Kostishyn, N.I. Zabeivorota, L.V. Panina, An V. Trukhanov, V.A. Turchenko, E.L. Trukhanova, V.V. Oleynik, O. S. Yakovenko, L. Yu Matzui, V.E. Zhivulin, High-frequency absorption properties of gallium weakly doped barium hexaferrites, Phil. Mag. (2018), https://doi.org/10.1080/14786435.2018.1547431.
[7] J. Song, S.A. Kulinich, J. Yan, Z. Li, J. He, C. Kan, H. Zeng, Epitaxial zno nanowire-on nanoplate structures as efficient and transferable field emitters, J. Adv. Mater. 25 (40) (2013) 5750–5755.
[8] H. Chen, C. Tan, D. Sun, W. Zhao, X. Tian, Y. Huang, Ultrawide range tuning of direct band gap in Mg-ZnO monolayer via electric field effect, RSC Adv. 8 (2018) 1392–1397.
[9] C. Pan, L. Dong, G. Zhu, S. Niu, R. Yu, Q. Yang, Y. Liu, Z.L. Wang, High-resolution electroluminescence imaging of pressure distribution using a piezo- electric nanowire led array, J. Nat. Photon 7 (2013) 752–758.
[10] V.A. Owoeye, E. Ajenifuja, E.A. Adeoye, A.O. Salau, S.A. Adewinbi, A.T. Akindadelo, D.A. Pelemo, A.P.I. Popoola, Effect of precursor concentration on corrosion resistance and microstructure of ZnO thin films using spray pyrolysis method, Scientific Africa Journal 15 (2022), e01073.

[11] A. O. Salau, A. S. Olufemi, G. l. Oluleye, V. A. Owoeye, I. Ismail, Modeling and performance analysis of dye-sensitized solar cell based on ZnO compact layer and TiO_2 photoanode, Journal of Materials Today: Proceedings, https://doi.org/10.1016/j.matpr.2021.05.592..

[12] A.V. Babalola, Effect of concentration and irradiation on the optical and structural properties of ZnO thin films deposited by spray pyrolysis techniques, J. Nucl. Inst. Methods Phys. Res. B 413 (2017) 57–61.

[13] M. Laurenti, V. Cauda, Porous zinc oxide thin films: synthesis approaches and applications, J. Coat. 8 (2018) 67.

[14] S. Muhamed, K.S. Saravana, K.V. Senthil, M.A. Uma, M. Sivakumar, R.M. Sreedevi, Enhancement of anticorrosion properties of stainless steel 304 L using nanostructured ZnO thin films, J. AIMS Mater. Sci. 5 (2018) 932–944.

[15] V.A. Owoeye, E. Ajenifuja, E.A. Adeoye, G.A. Osinkolu, A.P.I. Popoola, Microstructural and optical properties of Ni-doped ZnO thin films prepared by chemical spray pyrolysis technique, Mater. Res. Express 6 (2019), 086455.

[16] V.A. Owoeye, E. Ajenifuja, E.A. Adeoye, A.O. Salau, A.T. Akindadelo, D.A. Pelemo, A.P.I. Popoola, Microstructure and anti-corrosion properties of pray pyrolyzed Ni-doped ZnO thin films for multifunctional surface protection applications, Journal of Engineering Research Express 3 (2021), 025012.

[17] S. Ameen, M.S. Akhtar, H. Seo, Y.S. Kim, H.S. Shin, Influence of Sn doping on ZnO nanostructures from nanoparticles tospindleshape and their hotoelectrochemical properties for dye sensitizedsolar cells, Chem. Eng. J. 187 (2012) 351–356.

[18] N.D. Md Sin, M.H. Mamat, M. Rusop, Electrical properties of nanostructured aluminium doped zinc oxide (ZnO) thin film prepared using sol-gel spin coating methoid at different doping concentrations, Adv. Mater. Res. 666 (2013) 507–510.

[19] M. Ayachi, F. Ayad, A. Djelloul, L. Benharrat, S. Anas, Synthesis and chatracterization of Ni-doped ZnO thin films prepared by sol, -gelspin-coating method 55 (2021) 482–490.

[20] H. Layoul., F. Meriche., Y. Bouznit., A. Boukerika, Structure and Optical Characterization of Sol-Gel Processed Al-Doped ZnO Waveguide Films for ′integrated Optical Devices. doi.org/10.1007/s00339-021-04752-x.

[21] Yanfeng Wang, Guodong Xu, Jinzeng Yang, Weixi Mao, Jiankui Wang, Zhun Liu, Fabrication of AZO and FAZO films using low cost spin-coating method 124 (2022), 112204.

[22] Nur Hasyimah Hashim, Shanmugam Subramani, Mutharasu Devarajan, Structural and surface chaeacterization of undoped ZnO and Cu doped ZnO using sol-gel spin coating method, J. Mater. Sci. Mater. Electron. 27 (2016) 3520–3530.

[23] Andrew K. Rossall, Jaap A. van den Berg, David Meehan, Sudha Rajendiran, Erik Wagenaars, Analysis of Plasma Enhanced Pulsed Laser Deposition of Transition Metal Oxide Thin Films Using Medium Energy Ion Scattering, vol. 435, Elsevier, 2019, pp. 274–278.

[24] Babalola Adeoye Victor, Effect of Concentration and Irradiation on the Optical and Structural Properties of ZnO Thin Films Deposited by Spray Pyrolysis Techniques, vol. 413, Elsevier, 2017, pp. 57–61.

[25] S. Johnson Jeyakumar, J. Vasudevan, B. Arunkumar, M. Jothibas, A. Rajeswari, R. Sathiskumar, A. Muthuvel, Structural, optical and magnetic behavior of Sn doped ZnO nanoparticles prepared by solid state method, Mater. Today Proc. 48 (2022) 371–376, https://doi.org/10.1016/j.matpr.2020.09.376.

[26] A.L. Kozlovskiy, M.V. Zdorovets, Effect of doping of Ce4+/3+ on optical, strength and shielding properties of (0.5-x)TeO2-0.25MoO-0.25Bi2O3-xCeO2 glasses, Mater. Chem. Phys. 263 (2021), 124444.

[27] K.K. Kadyrzhanov, D.I. Shlimas, A.L. Kozlovskiy, M.V. Zdorovets, Research of the shielding effect and radiation resistance of composite CuBi2O4 flms as well as their practical applications, J. Mater. Sci. Mater. Electron. 31 (2020) 11729–11740.

[28] A.L. Kozlovskiy, M.V. Zdorovets, Synthesis, structural, strength and corrosion properties of thin flms of the type CuX (X=Bi, Mg, Ni), J. Mater. Sci. Mater. Electron. 30 (2019) 11819–11832.

[29] R.E. El-Shater, A.S. Atlam, M.K. Elnimr, S.T. Assar, S.V. Trukhanov, D.I. Tishkevich, T.I. Zubar, A.V. Trukhanov, D. Zhou, M.A. Darwish, AC measurements, impedance spectroscopy analysis, and magnetic properties of a multiferroic composite, Mater. Sci. Eng. B 286 (2022), 116025, https://doi.org/10.1016/j.mseb.2022.116025.

[30] N. Siva, D. Sakthi, S. Ragupathy, V. Arun, N. Kannadasan, Synthesis, structural, optical and photocatalytic behavior of Sn doped ZnOnanoparticles, Materials Science & Engineering B 253 (2020), 114497.

[31] S. Selvinsimpson, P. Gnanamozhi, V. Pandiyan, M. Govindasamy, M.A. Habila, N. AlMasoud, Y. Chen, Synergetic effect of Sn doped ZnO nanoparticles synthesized via ultrasonicationtechnique and its photocatalytic and antibacterial activity, Environ. Res. 197 (2021), 111115.

[32] M.V. Zdorovets, A.L. Kozlovskiy, D.I. Shlimas, D.B. Borgekov, Phase transformations in FeCo - Fe2CoO4/Co3O4-spinel nanostructures as a result of thermal annealing and their practical application, J. Mater. Sci. Mater. Electron. 32 (2021) 16694–16705, https://doi.org/10.1007/s10854-021-06226-5.

[33] O. Yakovenko, O. Lazarenko, L. Matzui, L. Vovchenko, M. Borovoy, P. Tesel'ko, O. Lozitsky, K. Astapovich, A. Trukhanov, S. Trukhanov, Effect of Ga content on magnetic properties of BaFe12-xGaxO19/epoxy composites, J. Mater. Sci. 55 (2020) 9385–9395, https://doi.org/10.1007/s10853-020-04661-z.

[34] M.A. Darwish, T.I. Zubar, O.D. Kanafyev, D. Zhou, E.L. Trukhanova, S.V. Trukhanov, A.V. Trukhanov, A.M. Henaish, Combined effect of microstructure, surface energy, and adhesion force on the friction of PVA/ferrite spinel nanocomposites, Nanomaterals 12 (2022) 1998, https://doi.org/10.3390/nano12121998.

[35] V.A. Owoeye, E. Ajenifuja, B. Babatope, G.A. Osinkolu, A.P.I. popoola, 0. popoola, experimental investigation and numerical simulation of mechanical properties and thermal stability of tin alloy processed by equal channel angular extrusion (ECAE), J. Eng. Res. Exp. 1 (2019), 025030.

[36] S.A. Adewinbi, W. Buremoh, V.A. Owoeye, Y.A. Ajayeoba, A.O. Salau, H.K. Busari, M.A. Tijani, B.A. Taleatu, Preparation and characterization of TiO_2 thin film electrode for optoelectronic and energy storage potentials: effects of Co incorporation, Chem. Phys. Lett. 779 (2021), 138854, https://doi.org/10.1016/j.cplett.2021.138854.

[37] A. Ali, E. Omotoso, J.M. Nel, W.E. Meyer, Electrical characterization of Au/Ni Schottky contacts on GaN synthesized using electrodeposition, Semicond. Sci. Technol. 38 (10pp) (2023), 045005.

[38] M.A. Ahmed, W.E. Meyer, J.M. Nel, Investigation of the structural and temperature dependent electrical properties of MZnO (M = Ce and Sm) Schottky diode devices fabricated using the sol–gel spin-coating technique, J. Mater. Sci. Mater. Electron. 34 (2023) 1312.

[39] E. Omotoso, W.E. Meyer, E. Igumbor, T.T. Hlatshwayo, A.R.E. Prinsloo, F.D. Auret, C.J. Sheppard, DLTS study of the influence of annealing on deep level defects induced in xenon ions implanted n-type 4H-SiC, J. Mater. Sci. Mater. Electron. 33 (2022) 15679–15688.

[40] Look, et al., Characterization of homoepitaxial p-type ZnO grown by molecular beam epitaxy, Appl. Phys. Lett. 81 (10) (2002) 1830–1832.

[41] Park, et al., Size control of ZnO nanorod arrays grown by metalorganic chemical vapour deposition, Nanotechnol 16 (10) (2005) 2044.

[42] Jin, et al., Violet and UV luminescence emitted from ZnO thin films grown on sapphire by pulsed laser deposition, Thin Solid Films 366 (1–2) (2000) 107–110.

[43] R.E. El-Shater, H. El Shimy, S.A. Saafan, M.A. Darwish, D. Zhou, A.V. Trukhanov, S.V. Trukhanov, F. Fakhry, Synthesis, characterization, and magnetic properties of Mn nanoferrites, J. Alloys Compd. 928 (2022), 166954, https://doi.org/10.1016/j.jallcom.2022.166954.

[44] A. Kotelnikova, T. Zubar, T. Vershinina, M. Panasiuk, O. Kanafyev, V. Fedkin, I. Kubasov, A. Turutin, S. Trukhanov, D. Tishkevich, V. Fedosyuk, A. Trukhanov, Saccharin adsorption influence on the NiFe alloy films growth mechanisms during electrodeposition, RSC Adv. 12 (2022) 35722–35729, https://doi.org/10.1039/D2RA07118E.

[45] E. Karakose, H. Çolak, Effect of substrate temperature on the structural properties of ZnO nanorods, Energy 141 (2017) 50–55.

[46] G. Ojeda-Barrero, A.I. Oliva-Avilés, A.I. Oliva, R.D. Maldonado, M. Acosta, G.M. Alonzo-Medina, Effect of the substrate temperature on the physical properties of sprayed-CdS films by using an automatized perfume atomizer, Mater. Sci. Semicond. Process. 79 (2018) 7–13.

[47] M.N. Amroun, M. Khadraoui, Effect of substrate temperature on the properties of SnS_2 thin films, Optik (2019), https://doi.org/10.1016/j.ijleo.2019.03.011.

[48] S. Venkataraj, S. Hishita, Y. Adachi, I. Sakaguchi, K. Matsumoto, N. Saito, H. Hanedaand N. Ohashi, Structure and electric properties in tin-doped zinc oxide films synthesized by pulsed laser deposition, J. Electrochem. Soc. 156 (6) (2009) H424–H429, https://doi.org/10.1149/1.3110892.

[49] S.V. Trukhanov, Magnetic and magnetotransport properties of La1-xBaxMnO3-x/2 perovskite manganites, J. Mater. Chem. 13 (2) (2003) 347–352. https://10.1039/b208664f.

[50] A. Kozlovskiy, K. Egizbek, M.V. Zdorovets, M. Ibragimova, A. Shumskaya, A.A. Rogachev, Z.V. Ignatovich, K. Kadyrzhanov, Evaluation of the efficiency of detection and capture of manganese in aqueous solutions of FeCeOx nanocomposites doped with Nb2O5, Sensors 20 (17) (2020) 4851. https://10.3390/s20174851.

[51] R. Ayouchi, D. Leinen, F. Martin, M. Gabas, E. Dalchiele, J. Ramos-Barrado, Preparation and characterization of transparent ZnO thin films obtained by spray pyrolysis 426 (2003) 68–77.
[52] J. Damisa, J.O. Emegha, XRD and UV-Vis Spectroscopic studies of lead tin sulphide (PbSnS) thin films, Trends in Sciences 18 (20) (2021) 1–11, https://doi.org/10.48048/tis.2021.16, 2021.
[53] I.A. Ezenwa, Synthesis and optical characterization of zinc oxide thin films, Res. J. Chem. Sci. 2 (2012) 26–30.
[54] J.O. Emegha, C.M. Okafor, K.E. Ukhurebor, Optical properties of copper-zinc sulphide network from mixed single solid source precursors of copper and zinc dithiocarbamate, Walaika J. Sci. & Tech 18 (9) (2021) 1–11.
[55] J.O. Emegha, K.E. Ukhurebor, U. Aigbe, B. Olofinjana, S.O. Azi, M.A. Eleruja, Effect of deposition temperature on the properties of copper-zinc sulphide thin films using mixed copper and zinc dithiocarbamate precursors, GU J Sci 35 (4) (2023) 1556–1570, https://doi.org/10.35378/gujs.887025, 2022.
[56] J.O. Emegha, K.E. Ukhurebor, U.O. Aigbe, J. Damisa, A.V. Babalola, Synthesis and characterization of copper zinc iron sulphide (CZFS) thin films, Heliyon 8 (2022), e10331.
[57] S. Aydogu, O. Sendil, M.B. Coban, The optical and structural properties of ZnO thin films deposited by the spray pyrolysis techniques, Chinese J Phys 50 (2012).
[58] N. Baydogan, H. Ozdurmusoglu, A. Cimenoglu, B. Tugrul, Refractive Index and Extinction Coefficient of ZnO:Al Thin Films Derived by Sol-Gel Dip Coating Technique, Defect and Diffusion Forum334, 2013, pp. 290–293.
[59] A. N. Orelusi, V. A. Owoeye, J. B. Dada, A. O. Salau, H. O. Boyo, S. A. Adewinbi, Investigation of microstructure and optical characteristics of Ti-doped ZnO thin films as an effective solar collector in photovoltaic solar cell applications using digitally controlled spray pyrolysis, J. Mater. Sci., DOI:10.1557/s43578-023-01133-3..
[60] F.Z. Bedia, A. Bedia, M. Aillerie, N. Mabufi, B. Benyoucef, Structural, optical and electrical properties of Sn-doped zinc oxide transparent films interesting for organic solar cells (OSC), Energy Proc. 74 (2015) 539–546.
[61] Z. Chen, D. Han, X. Zhang, Y. Wang, Improving performance of tin-doped-zinc-oxide thin-FilmTransistors by optimizing channel structure, Sci. Rep. 9 (2019) 17175, https://doi.org/10.1038/s41598-019-53766-2.
[62] E.S. Hassan, T.H. Mubarak, K.H. Abass, S.S. Chiad, N.F. Habubi, M.H. Rahid, A.A. Khadayeir, M.O. Dawod, I.A. Al-Baidhany, Structural,morphological and optical characterization of tin doped zinc oxide thin film by (SPT), J. Phys.: Conf. Ser. 1234 (2019), 012013.
[63] J.O. Emegha, K.E. Ukhurebor, E.O. Nonum, T.E. Arijaje, E. Danladi, T.C. Simon, Optoelectronic properties of chemically synthesized copper cadmium sulphide thin films,", J. Appl. Sci. Environ. Manage.. 26 (3) (2022) 385–392.
[64] S.V. Trukhanov, V.V. Fedotova, A.V. Trukhanov, S.G. Stepin, H. Szymczak, Synthesis and structure of nanocrystalline La0.50Ba0.50MnO3, Crystallogr. Rep. 53 (2008) 1177–1180, https://doi.org/10.1134/S1063774508070158.
[65] A.L. Kozlovskiy, A. Alina, M.V. Zdorovets, Study of the effect of ion irradiation on increasing the photocatalytic activity of WO3 microparticles, J. Mater. Sci. Mater. Electron. 32 (2021) 3863–3877, https://doi.org/10.1007/s10854-020-05130-8.